



A Machine Learning Framework With an Intelligent Algorithm for Predicting the Isentropic Efficiency of a Hydraulic Diaphragm Metering Pump in the Organic Rankine Cycle System

Xu Ping, Baofeng Yao*, Kai Niu and Meng Yuan

Key Laboratory of Enhanced Heat Transfer and Energy Conservation of MOE, Beijing Key Laboratory of Heat Transfer and Energy Conversion, Faculty of Environment and Life, Beijing University of Technology, Beijing, China

OPEN ACCESS

Edited by:

Enhua Wang,
Beijing Institute of Technology, China

Reviewed by:

Yongqiang Feng,
Jiangsu University, China
Bin Xu,
University of Oklahoma, United States
Huan Xi,
Xi'an Jiaotong University, China

*Correspondence:

Baofeng Yao
yaobf@bjut.edu.cn

Specialty section:

This article was submitted to
Process and Energy Systems
Engineering,
a section of the journal
Frontiers in Energy Research

Received: 10 January 2022

Accepted: 31 January 2022

Published: 16 February 2022

Citation:

Ping X, Yao B, Niu K and Yuan M
(2022) A Machine Learning Framework
With an Intelligent Algorithm for
Predicting the Isentropic Efficiency of a
Hydraulic Diaphragm Metering Pump
in the Organic Rankine Cycle System.
Front. Energy Res. 10:851513.
doi: 10.3389/fenrg.2022.851513

The pump provides the necessary pressure and flow for the organic Rankine cycle (ORC) system. The traditional methods have obvious limitations when analyzing the time-varying characteristics of the key operating parameters of the pump. This study first introduces the scatter plot analysis method to analyze and evaluate the time-varying and coupling characteristics of the hydraulic diaphragm metering pump. Then, a machine learning-fitting algorithm hybrid model is constructed to solve and verify the actual matching correlation equation of the key operating parameters. In addition, the complicated non-linear relationship brings great challenges to obtaining the limit value of the pump isentropic efficiency. This study introduces the bilinear interpolation algorithm to systematically analyze the change trend between operating parameters and isentropic efficiency. Based on the wavelet neural network (WNN) with momentum term and particle swarm optimization-adaptive inertia weight adjusting (PSO-AIWA), a machine learning framework with an intelligent algorithm is constructed. Under this framework, the maximum isentropic efficiency of the pump can be stabilized at 70.22–74.67% under all working conditions. Through the theoretical analysis model, the effectiveness of this framework is evaluated. Finally, the optimal cycle parameters are evaluated. This study can provide direct significance for the analysis and optimization of the actual performance of the ORC system.

Keywords: Organic Rankine cycle, Hydraulic diaphragm metering pump, Isentropic efficiency, Machine learning, Particle swarm optimization

Abbreviations: p , pressure (MPa); T , temperature ($^{\circ}$ C); \dot{m} , mass flow rate (kg/s); \dot{W} , power consumption (W); η , efficiency; t , time (s); in, inlet; out, outlet; s, isentropic; ORC, organic Rankine cycle; CCHP, combined cooling, heating and power; WNN, wavelet neural network; PSO-AIWA, particle swarm optimization-adaptive inertia weight adjusting; WHR, waste heat recovery; ANN, artificial neural network; BPNN, backpropagation neural network; RMSE, root mean square error.

1 INTRODUCTION

Energy is the foundation of economic development. The rapid economic development is accompanied by the massive consumption of energy, which makes the problem of energy shortage and environmental pollution increasingly severe. Globally, the widely distributed and huge amount of waste heat is not fully utilized (Xu et al., 2021). The development of the waste heat recovery (WHR) technology is conducive to improving the comprehensive utilization of energy.

The ORC plays an important role in the WHR field because of its high reliability and easy maintenance (Roumpedakis et al., 2019; Feng et al., 2020; Wang et al., 2022). The working fluid pump provides the necessary pressure for the ORC, which directly determines the performance of the system (Villani and Tribioli, 2019; Ping et al., 2021a; Ping et al., 2021b). The outlet pressure of the working fluid pump directly determines the evaporation pressure of the evaporator (Feng et al., 2015a; Wang et al., 2017a). As the outlet pressure of the working fluid pump increases, the inlet pressure of the expander also increases. At the same time, the thermal efficiency and net power output of the system are improved to varying degrees (Meng et al., 2017). In addition, the increase in evaporation pressure is conducive to improving the efficiency of the expansion engine (Ping et al., 2021c). Generally, in theoretical analysis and optimization, the circulation pressure and mass flow rate are matched through a linear relationship. However, there is a complicated nonlinear change relationship between circulation pressure and mass flow (Feng et al., 2015b; Li et al., 2020; D'Amico et al., 2018). Simple linear combination will ignore the objective nonlinear change relationship, which is not conducive to analysis and optimization.

Isentropic efficiency is one of the important evaluation indexes of the working fluid pump operating performance. The isentropic efficiency of the working fluid pump reflects the deviation between the enthalpy rise of ideal pressurization and the actual pressurization of the working fluid. Higher isentropic efficiency means that the working fluid pump has lower irreversible loss, and the corresponding ORC system has a

better overall performance (Uusitalo et al., 2020). In theoretical analysis, the isentropic efficiency usually takes a fixed value that has not been verified by experiments. **Table 1** briefly lists the selection of the isentropic efficiency of the pump (Mohammadzadeh Bina et al., 2017; Mateu-Royo et al., 2019; Shen et al., 2019; Wang and Fu, 2019; Altun and Kilic, 2020; Morais et al., 2020; Schiffelechner et al., 2020; Jafary et al., 2021; Khoshgoftar Manesh et al., 2021; Wang et al., 2021). The experimental test showed that the diaphragm pump efficiency was 32% (Kosmadakis et al., 2016); the efficiency of the vane pump was 36.9% (Kim et al., 2017); the plunger pump efficiency was 33.6% (Chang et al., 2015). From the above analysis, the difference between the theoretical analysis and the actual test of the pump isentropic efficiency is obvious. This makes the theoretical analysis insufficient for the ORC system performance evaluation and poor guidance for experimental research.

In addition, part of the theoretical analysis ignores the influence of the irreversibility of the working fluid pump pressurization process on the ORC system. Experiments show that there is an obvious correlation between the operating characteristics of the pump and the performance of the ORC system (Wang et al., 2017b). Miao et al. (2015) found that the peak power of the pump can account for 29.9% of the expander. Peris et al. (2015) analyzed the influence of the power consumption of the multistage centrifugal pump on the thermal efficiency of the system through the experiment. The results showed that the efficiency is 8.8% under the premise of considering the pump power consumption; without considering the pump power consumption, the thermal efficiency of the system can reach 10.64%. After testing the performance of the medium and low temperature ORC system, Wang et al. (2010) found that when the working fluid pump power consumption is not considered, the system thermal efficiency was 3.2%; when the working fluid pump power consumption was considered, the system thermal efficiency was only 1%. Moreover, the current research on pumps is generally carried out on the test bench of the ORC system (Feng et al., 2019). Because the experimental test of the ORC system is generally carried out under a stable high-

TABLE 1 | Isentropic efficiency in theoretical analysis.

Refs	Year	Research description	Isentropic efficiency (%)
Khoshgoftar Manesh et al. (2021)	2021	Thermodynamic modeling, simulation, and evaluation of the integrated cycle (supercritical carbon dioxide cycle and ORC) are performed	80
Jafary et al. (2021)	2021	Energetic and exergetic analysis of the ORC-internal heat exchange-based system	85
Wang et al. (2021)	2021	Design and optimization of the ORC for marine engine waste heat recovery	80
Morais et al. (2020)	2020	Economic, energetic, and exergetic analyses of a solar-biomass-ORC cooling cogeneration hybrid system	85
Altun and Kilic (2020)	2020	Thermodynamic evaluation of the ORC for geothermal power	80
Schiffelechner et al. (2020)	2020	Thermodynamic comparison of the supercritical CO ₂ and ORC for geothermal combined heat and power generation	80
Wang and Fu (2019)	2019	Thermoeconomic analysis of the CCHP-ORC system	80
Shen et al. (2019)	2019	Design and optimization of the ORC system	100
Mateu-Royo et al. (2019)	2019	Multi-objective optimization of a high-temperature heat pump-ORC hybrid system	90
Mohammadzadeh Bina et al. (2017)	2017	Thermoeconomic evaluation of the ORC for geothermal power	95

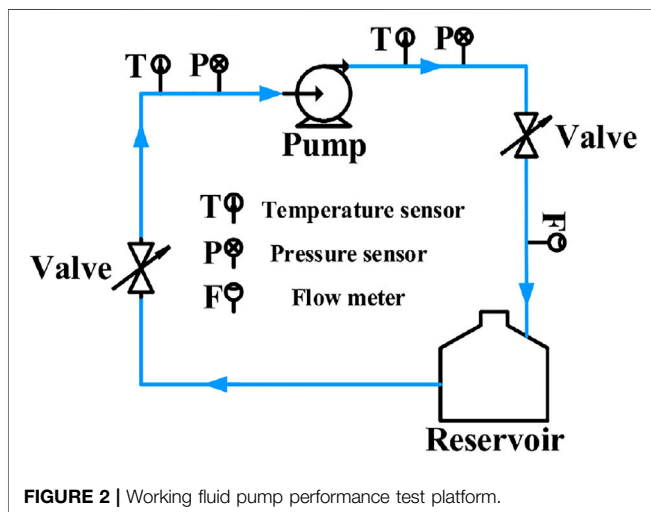
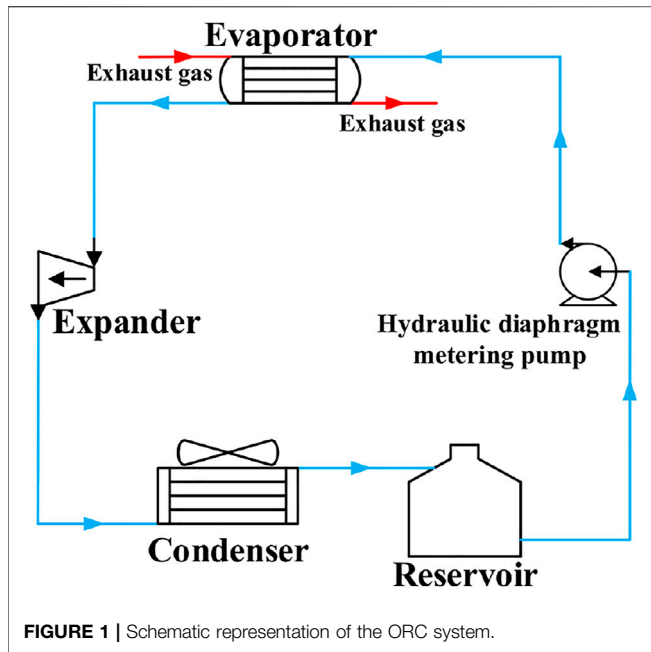
temperature heat source, the pump cannot be operated under full working conditions. The lack of some working conditions makes it impossible to analyze the coupling characteristics between the operating parameters and the isentropic efficiency in detail.

There are many operating parameters related to the isentropic efficiency of the working fluid pump, and the interaction is complicated. Moreover, there is a relatively obvious nonlinear relationship between the isentropic efficiency and the operating parameters. Conventional analysis methods have limitations in constructing the nonlinear dynamic characteristics of the working fluid pump. In recent years, machine learning has provided new ideas and methods for solving the dynamic characteristic modeling problems related to the ORC. Palagi et al. (2019) compared the predictive accuracy of the ORC system feedforward, recurrent, and long short-term memory network models. Rossi and Renzi (2018) constructed an ANN prediction model for the pump. By evaluating the robustness, the feasibility of using ANN to construct pump dynamic characteristics is verified. Fubin Yang et al. (2018) first built a neural network model based on the characteristics of the data. Then, through a genetic algorithm, the robustness of the model was improved. The maximum net power output of the system was 7.13 kW; the prediction error of the model was between -0.2 and 0.2 kW. Zhao et al. (2019) optimized the ORC system performance globally. After optimization by the particle swarm algorithm, the net power output of the system exceeds 6.87% of the initial net power output of the system. Ping et al. (2020), Ping et al. (2021d) analyzed and evaluated the nonlinear relationship between the key component parameters and performance in the ORC system through machine learning and intelligent algorithms. Then, the performance of key components was predicted and optimized. It can be seen that in the dynamic characteristic modeling of the ORC system, machine learning has an excellent learning ability, parallel computing ability, and adaptability to a large amount of information. This feature not only provides a new method for solving the dynamic characteristic matching of key parameters but also brings new ideas for predicting the isentropic efficiency. The wavelet neural network is composed of the wavelet transform theory and neural network. The wavelet basis function is the activation function in the neural network. At the same time, the factors in the basis functions replace the thresholds in the hidden layer nodes. Therefore, this structure fundamentally changes the topology of the BPNN. Based on the wavelet theory, the parameters and structure of the model are initialized. Therefore, from the perspective of a fitting performance, the wavelet transform function can be selected according to the characteristics of the fitted variable. Therefore, the WNN has strong robustness, generalization ability, and convergence speed. In addition, the wavelet transform function has orthogonality. Therefore, the wavelet transform function can select the best strategy to fit the objective function. The WNN not only has the generalization ability of a neural network but also has the multi-scale analysis ability of wavelet transform (Yuan et al., 2020; Hamedani et al., 2021; Jafarzadeh Ghouschi et al., 2021). The selection of inertia weight has an important effect on PSO. Inertia weight can effectively adjust the influence of the last search speed on the

next search speed. Inertia weight can also effectively balance the relationship between the local search and global search in PSO. Larger inertia weight will improve the global search capability of the algorithm. The smaller inertia weight is beneficial to the local search of the algorithm, which improves the local search ability and speeds up the convergence of the algorithm. In the conventional PSO algorithm, the inertia weight decreases linearly with the number of iterations. When the algorithm has obtained the global optimal value in the early stage, the inertia weight cannot be reduced quickly, so the algorithm cannot realize the local search. When the algorithm is in the local optimization, this method cannot effectively avoid the local optimal value. Therefore, in order to make the algorithm search for the maximum value of the isentropic efficiency quickly and effectively, this study introduces the PSO-AIWA algorithm. The inertia weight is not affected by the number of iterations, so the local search ability and global search ability of the algorithm are balanced. Therefore, the PSO-AIWA algorithm can improve the convergence accuracy of the algorithm while ensuring the diversity of particle swarm (Wu et al., 2014; Taherkhani and Safabakhsh, 2016; Hop et al., 2021).

A positive displacement pump is widely concerned in the ORC field because of its good sealing and easy maintenance (Nematollahi et al., 2018; Wang et al., 2019; Carraro et al., 2020). As a kind of the positive displacement pump, the hydraulic diaphragm metering pump has a better metering accuracy than the mechanical diaphragm pump and a better sealing performance than the plunger pump. In this study, the scatter plot analysis method is introduced to analyze the time-varying characteristics of the key operation parameters in the visualization plane. This study introduces the scatter plot analysis method and the bilinear interpolation algorithm to analyze time-varying characteristics of the key operating parameters and the change trend of isentropic efficiency under all working conditions. In addition, a machine learning model for matching the key operating parameters is constructed. The model is coupled with a fitting algorithm into a machine learning-fitting algorithm hybrid model, which solves and verifies the actual matching correlations of the key operating parameters. Moreover, based on a wavelet neural network (WNN) with the momentum term, an isentropic efficiency machine learning prediction model is constructed. The model and the particle swarm optimization-adaptive inertia weight adjusting (PSO-AIWA) are coupled into a machine learning framework with an intelligent algorithm. Then, through the theoretical analysis model, the effectiveness of the machine learning model is verified. Finally, the isentropic efficiency limiting and optimal cycle parameters are evaluated.

The key operating parameter matching correlation equation of the hydraulic diaphragm metering pump takes into account the nonlinear mapping relationship between operating parameters and time-varying characteristics, which provides useful guidance for the theoretical analysis, experimental design, and component matching of the ORC system. Obtaining the maximum value of the isentropic efficiency of the hydraulic diaphragm metering pump under different working conditions is conducive to the selection of numerical values in theoretical calculations.

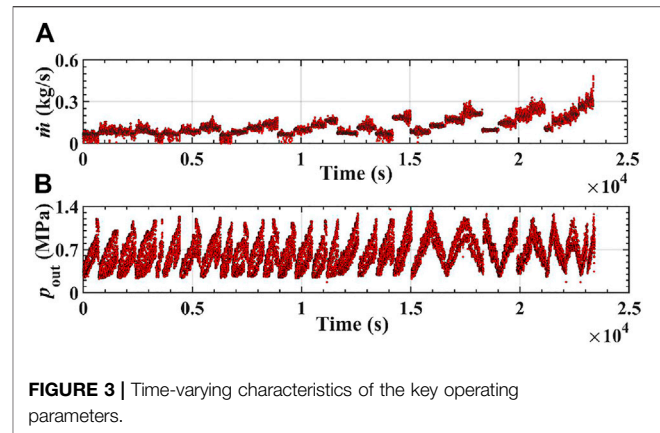


Moreover, it also brings direct guidance for obtaining the ORC system performance limits.

2 DYNAMIC CHARACTERISTICS

2.1 Bench Description

Yuxin Yang et al. (2018) have described the bench of the hydraulic diaphragm metering pump in detail. This study introduces the ORC system and working conditions of the pump. The ORC system is shown in **Figure 1**. The speed of the hydraulic diaphragm metering pump can be changed by the frequency converter. The working conditions selected in this study need to cover the entire working condition range as



comprehensively as possible in order to systematically optimize the isentropic efficiency. We selected 15, 20, 25, 30, 35, 40, 45, and 50 Hz at equal intervals in the full frequency band that the motor can cover. The corresponding hydraulic diaphragm metering pump speeds are 870 r/min–2900 r/min.

2.2 Matching Characteristics

A performance test platform for the hydraulic diaphragm metering pump is established using R245fa as the organic fluid, and the performance of the pump under different working conditions is tested. **Figure 2** is the schematic diagram of the working fluid pump performance test platform. The experimental process is as follows: first, make sure that the components in the test platform are connected to the pipeline tightly. The liquid storage tank and pipeline in the test platform are evacuated, and R245fa is added to the liquid storage tank. The working fluid enters the pump from the tank and is pressurized in the pump. The valve can adjust the flow, thus changing the circulation pressure. Finally, the working fluid re-enters the liquid storage tank to complete the cycle. The frequency converter is used to control the speed of the working fluid pump. A power sensor is used to measure the power consumption of the working fluid pump. The flowmeter is used to measure the flow of the working fluid. The flowmeter is located behind the valve at the outlet of the working fluid pump. The experimental data in the cycle are collected by using the data acquisition instrument.

In the actual operation process of the hydraulic diaphragm metering pump, the operating parameters have transient pulsation. This characteristic makes the key operating parameters have strong time-varying characteristics. **Figure 3A** shows the time-varying characteristics of the mass flow rate. The figure shows that there is a strong correlation and periodicity between the mass flow rate and time, and the mass flow rate can be regarded as a time series variable. **Figure 3B** shows the time-varying characteristics of the outlet pressure. From the figure, although the outlet pressure changes frequently, it has a strong correlation and periodicity with time. The outlet pressure can be regarded as a time series variable. Therefore, the construction of time series correlations will help to obtain actual matching correlations between the key operating parameters.

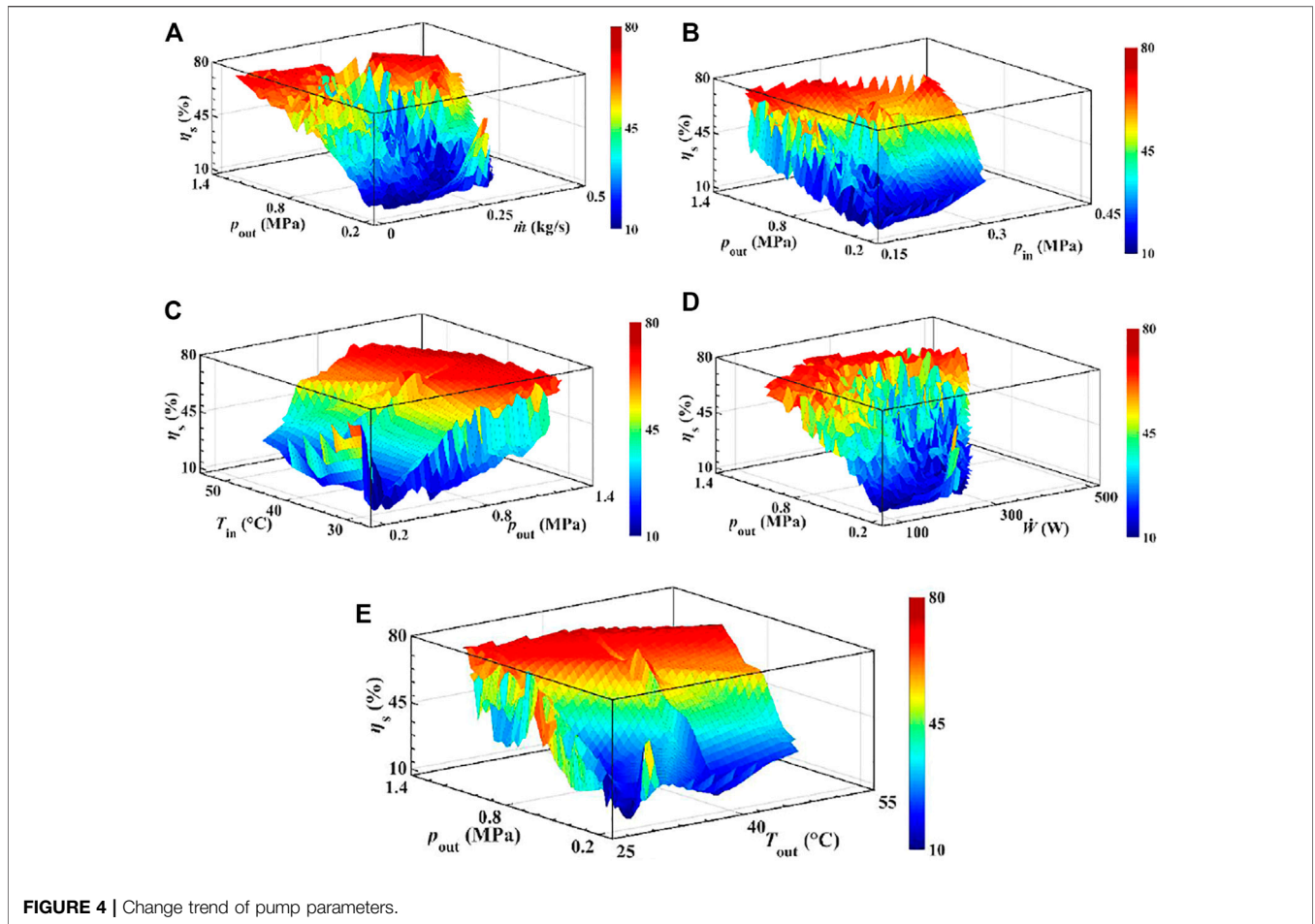


FIGURE 4 | Change trend of pump parameters.

2.3 Isentropic Efficiency

The transient characteristic also makes the isentropic efficiency and operating parameters have a strong nonlinear dynamic characteristic. Different operating parameters have obvious differences in the effect of isentropic efficiency. In this study, the bilinear interpolation algorithm is used to fit the mapping relationship between the operating parameters and isentropic efficiency, and the influence surface of different operating parameters on isentropic efficiency is drawn in a three-dimensional space. Based on the fitting surface, the nonlinear variation trend between the operating parameters and isentropic efficiency is analyzed. The bilinear interpolation algorithm interpolates the data points in different dimensions and then combines the data points in different dimensions. This feature can not only fully consider the change relationship between adjacent data points but also reduce the calculation cost. For given points A (i, j), B (i + 1, j), C (i, j + 1), and D (i + 1, j + 1) on the plane, the corresponding isentropic efficiencies are $\eta_s(i, j)$, $\eta_s(i + 1, j)$, $\eta_s(i, j + 1)$, and $\eta_s(i + 1, j + 1)$. The point to be interpolated is P (i + u, j + v), and the corresponding isentropic efficiency is $\eta_s(i + u, j + v)$. Here, u and v are the increments in the X-axis and Y-axis directions, respectively. Then, the isentropic efficiencies corresponding to E (i + u, j) and F (i + u, j + 1) can be expressed as follows:

$$\eta_s(i + u, j) = \eta_s(i, j) + u[\eta_s(i + 1, j) - \eta_s(i, j)], \quad (1)$$

$$\eta_s(i + u, j + 1) = \eta_s(i, j + 1) + u[\eta_s(i + 1, j + 1) - \eta_s(i, j + 1)], \quad (2)$$

$\eta_s(i + u, j + v)$ can be expressed as follows:

$$\eta_s(i + u, j + v) = \eta_s(i + u, j) + v[\eta_s(i + u, j + 1) - \eta_s(i + u, j)], \quad (3)$$

Figure 4 shows the fitting results of the bilinear interpolation algorithm. It can be seen from **Figure 4A** that as the outlet pressure increases, the isentropic efficiency gradually increases. Starting from the outlet pressure around 0.87 MPa, the isentropic efficiency increases slightly. As the mass flow rate increases, the isentropic efficiency generally shows an increasing trend, but the increase is not obvious. In addition, the outlet pressure has a greater impact on the isentropic efficiency than the mass flow rate. It can be seen from **Figure 4B** that the isentropic efficiency gradually increases as the inlet pressure increases. Compared with the inlet pressure, the outlet pressure has a greater impact on the isentropic efficiency. Starting from the inlet pressure around 0.25 MPa, the isentropic efficiency increases slightly. From **Figure 4C**, the isentropic efficiency does not increase significantly with the increase of the inlet temperature. From

Figure 4D, as power consumption increases, the isentropic efficiency decreases. From **Figure 4E**, the isentropic efficiency increases with the increase of the outlet temperature before 32°C. Starting from the outlet temperature around 32°C, the isentropic efficiency increases mildly.

3 MACHINE LEARNING

3.1 WNN and PSO

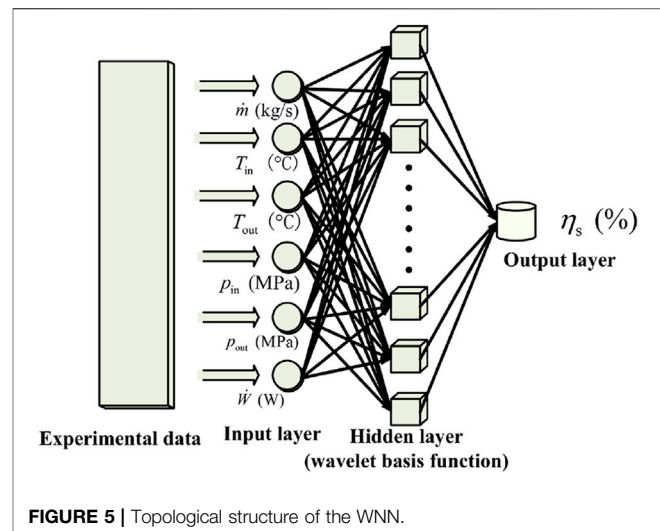
The WNN has the advantages of the ANN and wavelet analysis at the same time; the network has fast convergence speed and has a strong ability to analyze transient processes (Santhosh et al., 2018; Guo et al., 2019; Yuan et al., 2020). The wavelet basis function is used as the activation function of the WNN, and the translation and expansion are performed through the translation factor and the expansion factor. The WNN is used to learn the dynamic operating characteristics of the hydraulic diaphragm metering pump so as to construct a nonlinear mapping relationship between the operating parameters and isentropic efficiency. Because the WNN uses the gradient learning algorithm to modify the weights and parameters, the learning progress of the WNN is slow, and it is easy to fall into local minimum. This study introduces the WNN with a momentum term to improve its learning efficiency.

The PSO algorithm has a strong ability of optimization. But in the process of optimization, the PSO algorithm is easy to produce a convergence effect of the population, causing premature and stagnation. In order to balance the local and global search capabilities of the PSO algorithm, this study introduces the PSO-AIWA algorithm.

The model construction process is as follows: machine learning first constructs a nonlinear mapping relationship by mining the characteristics of the training set and then, through the test set to evaluate its generalization ability. In addition, the 20,000 learning rate combinations and the 88 node numbers in the model structure under full working conditions are optimized and selected to further improve the generalization ability of the model.

Coupling the WNN with the momentum term and PSO-AIWA into a machine learning framework with an intelligent algorithm. The machine learning framework consists of two parts: prediction and optimization. The WNN model is used to predict the isentropic efficiency of the working fluid pump. The PSO-AIWA algorithm is used to optimize the isentropic efficiency of the working fluid pump. The output variable of the prediction model is used as the fitness function of the optimization algorithm. The fitness value of the optimization algorithm is the isentropic efficiency of the working fluid pump. The input variables of the prediction model are taken as the optimization variables of the optimization algorithm. By coupling the prediction model and optimization algorithm, the limit value of the isentropic efficiency of the working fluid pump is predicted and optimized.

Then, the isentropic efficiency limiting value of the hydraulic diaphragm metering pump under all working conditions is



optimized. The schematic representation of the WNN topology is shown in **Figure 5**.

3.2 BPNN

The BPNN has a solid theoretical foundation, good intelligence characteristics, and adaptability to off-line data. In the prediction model of the ORC system, the BPNN based on the error backpropagation algorithm is widely concerned. The BPNN can learn from a large number of input variables and output variables. In the process of learning, the BPNN can dynamically adjust weights and thresholds in the network so as to learn the mapping relationship. First, the neurons in the input layer transmit the acquired information to the hidden layer, and the hidden layer transmits the information to the output layer after transformation processing. The network then compares the deviation between the desired value and the actual value. Based on the deviation, the network propagates the error signal back to the input layer from back to front in the direction of the negative gradient. At the same time, the weights and thresholds in the network will be corrected. In the process of forward transmission of input information and reverse transmission of errors, the accuracy of the network is gradually improved (Hu et al., 2019; Wang et al., 2020; Xie et al., 2020).

Based on the characteristics of the BPNN, the mass flow rate time series prediction model and the outlet pressure time series prediction model are constructed, respectively. Then, the time series is predicted and evaluated.

3.3 Variable Selection

The isentropic efficiency prediction and optimization model selects the temperature, pressure, power consumption, and mass flow rate of the hydraulic diaphragm metering pump as input variables. The isentropic efficiency is the output variable.

The input variable of the mass flow rate time-varying characteristic prediction model is the equipment running time, and the output variable is the mass flow rate. The input variable of the time-varying characteristic prediction model of outlet

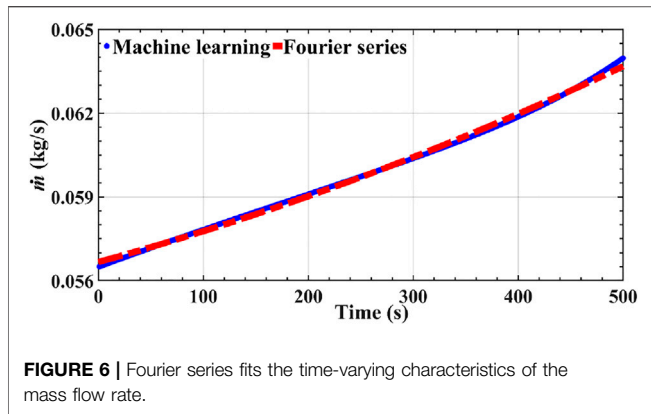


FIGURE 6 | Fourier series fits the time-varying characteristics of the mass flow rate.

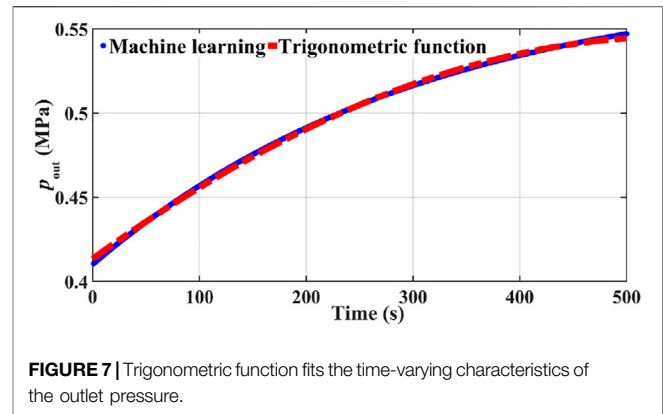


FIGURE 7 | Trigonometric function fits the time-varying characteristics of the outlet pressure.

pressure is the equipment running time, and the output variable is the outlet pressure.

4 RESULTS AND DISCUSSION

4.1 Model Evaluation

The evaluation of key operating parameter matching refers to the quantitative evaluation of the time-varying characteristic prediction and fitting ability of the hybrid model. The evaluation of the predictive model refers to the quantitative evaluation of the predictive ability.

Root mean square error (RMSE) represents the degree of deviation of the data set. The smaller the RMSE, the better will be the accuracy of the model. In this study, the RMSE is used to evaluate the accuracy. The RMSE is calculated as follows:

$$RMSE = \sqrt{\frac{1}{N} \sum_{i=1}^N (\text{observed}_i - \text{predicted}_i)^2}, \quad (4)$$

In the evaluation of key operating parameter matching, observed_i refers to the result obtained through the fitting algorithm. predicted_i refers to the result obtained through machine learning. In the evaluation of the isentropic efficiency limiting value prediction model, observed_i refers to the isentropic efficiency obtained through experimental data. predicted_i refers to the result of the isentropic efficiency predicted by the machine learning framework with the intelligent algorithm.

4.2 Key Operating Parameter Matching

The coefficients and constant terms of the final correlation equation are obtained by the BPNN, Fourier series fitting algorithm, and trigonometric function fitting algorithm. First, the time-varying characteristics of the mass flow rate and the outlet pressure of the working fluid pump are predicted by the BPNN. Then, the Fourier series fitting algorithm is used to fit the time-varying characteristics of the mass flow rate. The trigonometric function fitting algorithm is used to fit the time-varying characteristics of the outlet pressure. Finally, the key operating parameter-matching correlation is obtained through

the time-varying characteristic equation of the mass flow rate and the time-varying characteristic equation of the outlet pressure.

First, the time-varying characteristics of the mass flow rate are predicted. Then, the time-varying characteristics of the mass flow rate are fitted by the Fourier series, Gaussian function, ordinary least squares, power function, rational function, and trigonometric function. According to the prediction and fitting results, the RMSEs of Fourier series, Gaussian function, ordinary least squares, power function, rational function, and trigonometric function are 8.89×10^{-5} , 5.49×10^{-4} , 1.65×10^{-4} , 1×10^{-3} , 2.6×10^{-3} , and 2.08×10^{-4} , respectively. Therefore, the Fourier series fitting algorithm is used to fit the time-varying characteristics of the mass flow rate. **Figure 6** shows the fitting results of the Fourier series on the time-varying characteristics of the mass flow rate. The correlation between the mass flow rate and time is as follows:

$$\dot{m} = 2 - 2 \cos(10^{-2}t) + 10^{-1} \sin(10^{-2}t), \quad (5)$$

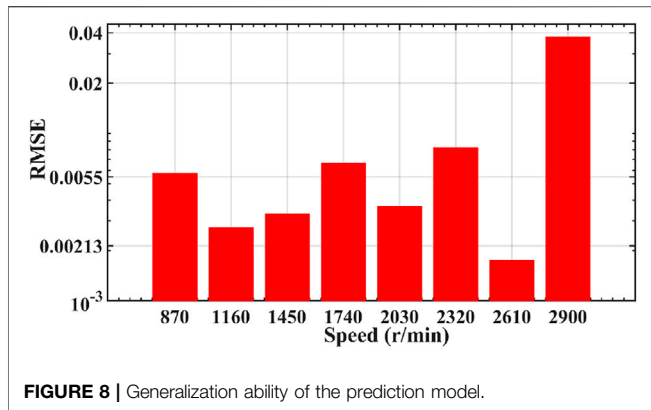
In addition, the time-varying characteristics of the outlet pressure are predicted. Then, the time-varying characteristics of the outlet pressure are fitted by Fourier series, Gaussian function, ordinary least squares, power function, rational function, and trigonometric function. According to the prediction and fitting results, the RMSEs of Fourier series, Gaussian function, ordinary least squares, power function, rational function, and trigonometric function are 2.49×10^{-2} , 1.5×10^{-3} , 7.8×10^{-3} , 1.1×10^{-2} , 4.02×10^{-2} , and 1.1×10^{-3} , respectively. Therefore, the trigonometric function fitting algorithm is used to fit the time-varying characteristics of the outlet pressure. **Figure 7** shows the fitting results of the trigonometric function on the time-varying characteristics of the outlet pressure. The correlation between the outlet pressure and time is as follows:

$$10 \arcsin(2p_{\text{out}}) - 9 = 10^{-2}t, \quad (6)$$

From **Eq. 5** and **Eq. 6**, we obtain the following:

$$\dot{m} = 2 - 2 \cos[10 \arcsin(2p_{\text{out}}) - 9] + 10^{-1} \sin[10 \arcsin(2p_{\text{out}}) - 9], \quad (7)$$

Equation 7 is the actual matching correlation equation for the key operating parameters of the hydraulic diaphragm metering pump.



rate of the wavelet basis function in the network is particularly important. Furthermore, the nodes in the network also have an important influence on the generalization ability of the network. The 20,000 learning rate combinations and 88 nodes are optimized to improve the generalization ability. **Table 2** lists the optimization results. From **Figure 8**, the RMSEs are 5.8×10^{-3} , 2.8×10^{-3} , 3.3×10^{-3} , 6.7×10^{-3} , 3.7×10^{-3} , 8.3×10^{-3} , 1.8×10^{-3} , and 3.8×10^{-2} , respectively. The prediction model has good generalization ability under full working conditions. In addition, the selection results of hyperparameters in the BPNN are also listed in **Table 2**.

4.3 Isentropic Efficiency Limiting Value

As we all know, the change of operating parameters of the hydraulic diaphragm metering pump directly affects the isentropic efficiency. Moreover, the strong coupling between the operating parameters and performance makes the degree of influence difference obvious. Although the experiment can test the isentropic efficiency of the hydraulic diaphragm metering pump, it is difficult to obtain the limiting value of the isentropic efficiency from limited and discrete experimental points. The research on transient pulsation characteristics of the pump is expensive and complicated. Theoretical analysis has great limitations for constructing the complex non-linear mapping relationship. Based on the WNN with the momentum term, an isentropic efficiency prediction model is constructed. Then, the model and the PSO-AIWA algorithm are coupled into a machine learning framework with the intelligent algorithm to optimize the isentropic efficiency. Within the boundaries of operating parameters, the limiting value under all working conditions is obtained.

4.3.2 Prediction and Optimization

In the experiment, a variety of operating parameters are constantly changing with the high-speed operation of the hydraulic diaphragm metering pump. There may be multiple maximum points of the isentropic efficiency in the region within the operating parameter boundaries. Therefore, it is necessary to make a reasonable selection of the optimization boundaries of the operating parameters so that the process of prediction and optimization is accurate and fast.

4.3.1 Generalization Ability

Structural parameters have an important influence on the generalization ability of the prediction model. Therefore, the selection of the learning rate of the weights and the learning

The bilinear interpolation algorithm is used to construct the curved surface to provide the required boundaries for prediction and optimization. The three dimensions in the space represent different operating parameters, and the fourth dimension represents the isentropic efficiency with the intensity of the color. The dark region is the region where the maximum isentropic efficiency may exist. **Figure 9** shows the region where the maximum isentropic efficiency may exist at 870 r/min. The optimization boundaries of the inlet pressure are 0.16–0.17 MPa; the optimization boundaries of the outlet temperature are 28.96–29.62°C; the optimization boundaries of the outlet pressure are 0.98–1.23 MPa; the optimization boundaries of power consumption are 120.55–195.7 W; the optimization boundaries of the mass flow rate are 0.066–0.072 kg/s; the optimization boundaries of the inlet temperature are 28.52–28.94°C.

TABLE 2 | Structural parameters of the WNN prediction model and BPNN prediction model.

Structural parameters of the WNN prediction model				
Speed (r/min)	Weights learning rate	Learning rate of wavelet basis function	Number of hidden layer nodes	Number of hidden layers
870	0.099	0.025	26	1
1160	0.081	0.077	22	1
1450	0.099	0.081	20	1
1740	0.091	0.001	12	1
2030	0.065	0.037	20	1
2320	0.063	0.051	12	1
2610	0.095	0.075	24	1
2900	0.025	0.015	18	1
Structural parameters of the BPNN prediction model				
Learning rate		Number of hidden layer nodes		Number of hidden layers
0.1		30		1

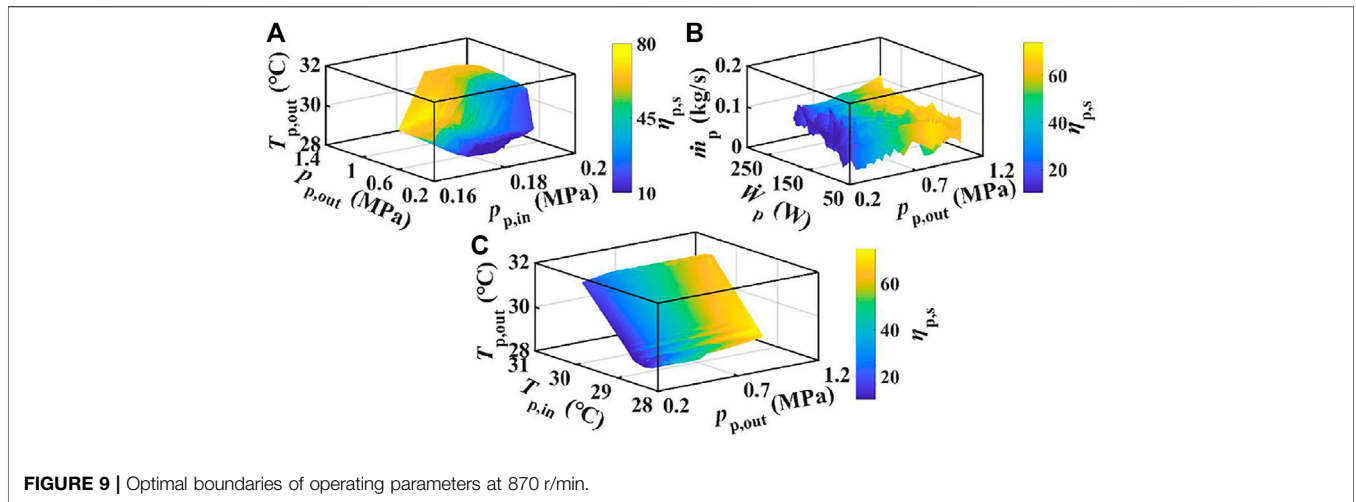


FIGURE 9 | Optimal boundaries of operating parameters at 870 r/min.

TABLE 3 | Constraints of the optimization process.

Speed (r/min)	T _{in} (°C)		T _{out} (°C)		ṁ (kg/s)		P _{in} (MPa)		P _{out} (MPa)		Ẇ (W)	
	Min	Max	Min	Max	Min	Max	Min	Max	Min	Max	Min	Max
870	28.52	28.94	28.96	29.62	0.07	0.07	0.17	0.18	0.98	1.23	120.5	195.7
1160	30.11	30.66	30.68	32.25	0.06	0.06	0.18	0.19	1.21	1.33	210.8	223.6
1450	28.95	29.34	29.36	29.81	0.1	0.12	0.18	0.19	0.91	0.95	129.1	138.2
1740	28.62	29.06	29.37	31.64	0.08	0.11	0.17	0.18	0.84	0.97	141.5	180.9
2030	29.17	29.54	29.96	30.5	0.06	0.07	0.18	0.19	1.04	1.23	200.5	220.3
2320	28.48	29.09	29.11	30.18	0.11	0.12	0.17	0.18	1.15	1.32	289.4	315.8
2610	27.36	28.45	28.71	30.01	0.09	0.11	0.18	0.19	1.25	1.47	227.6	245.4
2900 case1	38.86	40.21	40.27	41.67	0.32	0.36	0.26	0.27	1.15	1.32	357	395.4
2900 case2	52.38	52.67	52.77	53.13	0.27	0.29	0.34	0.38	0.9	1.05	381.2	390.6

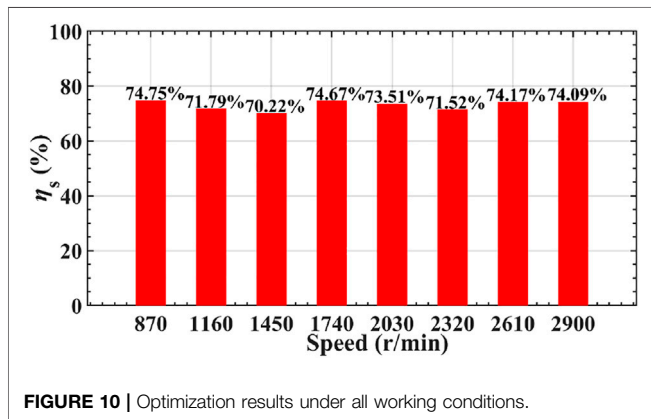


FIGURE 10 | Optimization results under all working conditions.

The cost function of this study can be expressed as follows:

$$\max(\eta_s) = f(\dot{m}, T_{in}, T_{out}, P_{in}, P_{out}, \dot{W}), \tag{8}$$

The inlet temperature, inlet pressure, outlet temperature, outlet pressure, power consumption, and mass flow of the hydraulic diaphragm metering pump are selected as the control variables in the process of optimization. The

boundary of control variables is constrained in the process of optimization. Constraints are shown in Table 3.

Figure 10 shows the optimization results of the maximum isentropic efficiency. The limiting value of the isentropic efficiency at 870–2900 r/min can be stabilized at 70.22–74.75%. Table 4 shows the optimal operating parameters corresponding to the isentropic efficiency limiting value under all working conditions. The results show that there is no unique set of speed and operating parameters to make the isentropic efficiency reach the limiting value under full working conditions. By reasonably adjusting the operating parameters, the isentropic efficiency of the hydraulic diaphragm metering pump can reach a larger value under different working conditions. Reasonable adjustment of different operating parameters through this framework can make the isentropic efficiency reach the maximum under all working conditions.

4.3.3 Verification and Comparison

Within the same optimization boundaries, the isentropic efficiency is optimized through theoretical analysis to verify the effectiveness of this framework. The prediction and optimization accuracy of the machine learning framework and theoretical analysis model are compared.

TABLE 4 | Optimal operating parameters.

Speed (r/min)	T _{in} (°C)	T _{out} (°C)	ṁ (kg/s)	p _{in} (MPa)	p _{out} (MPa)	Ẇ (W)
870	28.52	29.62	0.07	0.18	0.98	120.55
1160	30.11	32.25	0.06	0.19	1.21	223.6
1450	29.34	29.36	0.10	0.19	0.91	129.1
1740	28.62	31.52	0.09	0.18	0.84	177.89
2030	29.17	30.5	0.066	0.19	1.28	202.44
2320	28.48	30.19	0.12	0.17	1.15	289.4
2610	27.36	30.01	0.11	0.18	1.25	239.01
2900	38.86	40.83	0.32	0.27	1.15	369.02

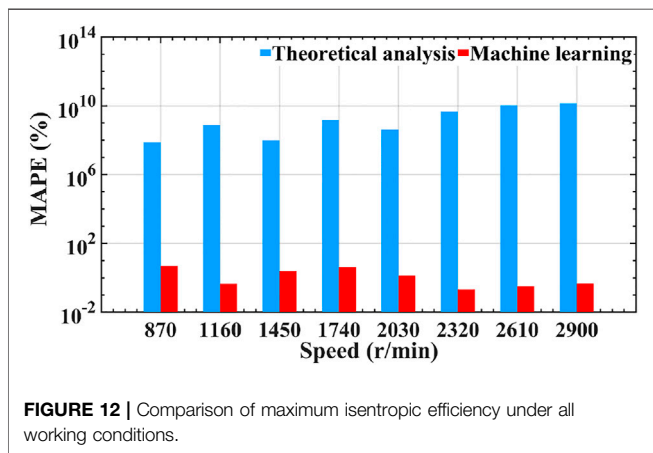
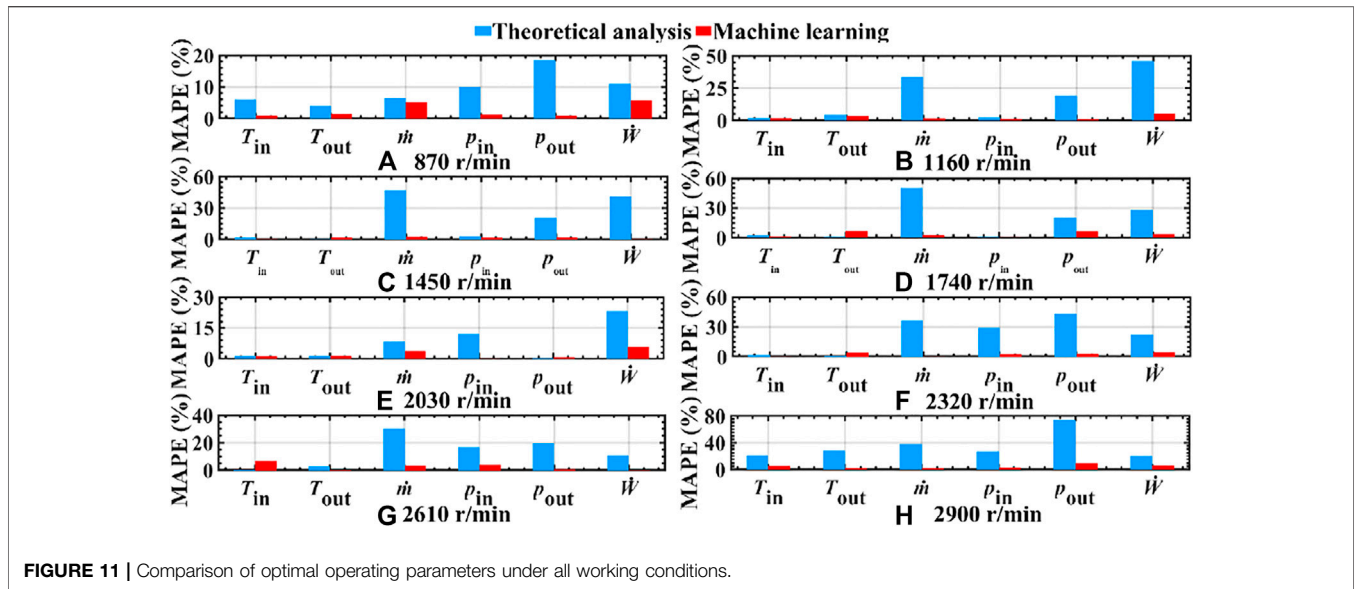
TABLE 5 | Differences between theoretical analysis modeling and machine learning modeling.

Theoretical analysis modeling		Machine learning modeling
Basic concept	According to the theoretical calculation equation and REFPROP, the changing relationship between operating parameters and performance is constructed	Wavelet transform is combined with the neural network. The neuron activation function is replaced by the nonlinear wavelet function
Key equation	$\eta_s = \frac{h_{s,out} - h_n}{T_{out} - T_{in}}$ (9)	Wavelet basis function: $y = \cos(1.75x)e^{-x^2}$ (10) Output layer calculation equation: $y(k) = \sum_{i=1}^m w_{ik}h(i)$ $k = 1, 2, \dots, m$ (11) Here, w_{ik} is the weight from the hidden layer to the output layer. $h(i)$ is the output of the i hidden layer node. I is the number of hidden layer nodes. m is the number of nodes in the output layer The correction of the wavelet network can be expressed as 1) Calculate the network error $e = \sum_{k=1}^m yn(k) - y(k)$ (12) Here, $yn(k)$ is the desired output. $y(k)$ is the prediction output of the wavelet neural network 2) Modify the weight of the wavelet neural network and the coefficient of basis function $w_{n,k}^{(i+1)} = w_{n,k}^i + \Delta w_{n,k}^{(i+1)}$ (13) $a_k^{(i+1)} = a_k^i + \Delta a_k^{(i+1)}$ (14) $b_k^{(i+1)} = b_k^i + \Delta b_k^{(i+1)}$ (15) Here, $\Delta w_{n,k}^{(i+1)} = -\eta \frac{\partial e}{\partial w_{n,k}^{(i+1)}}$ (16) $\Delta a_k^{(i+1)} = -\eta \frac{\partial e}{\partial a_k^{(i+1)}}$ (17) $\Delta b_k^{(i+1)} = -\eta \frac{\partial e}{\partial b_k^{(i+1)}}$ (18) Here, η is the learning rate

Table 5 shows the differences between theoretical analysis modeling and machine learning modeling. It can be seen from the table that the theoretical analysis is to calculate the efficiency of the pump through the theoretical calculation equation and REFPROP. First, the optimization algorithm generates a set of operating parameters. The enthalpy values corresponding to operating parameters are calculated by REFPROP in theoretical analysis. Then, the isentropic efficiency is calculated by the theoretical calculation equation. The output variables of the theoretical analysis model are taken as the fitness function of the optimization algorithm. The fitness value of the optimization algorithm is the isentropic efficiency of the pump. The input variables of the theoretical analysis model are taken as the optimization variables of the optimization algorithm. The theoretical analysis model is coupled with the optimization algorithm to optimize the isentropic efficiency of the pump. The machine learning model is composed of the wavelet transform and neural network, which can directly construct

the mapping relationship between the operating parameters and isentropic efficiency.

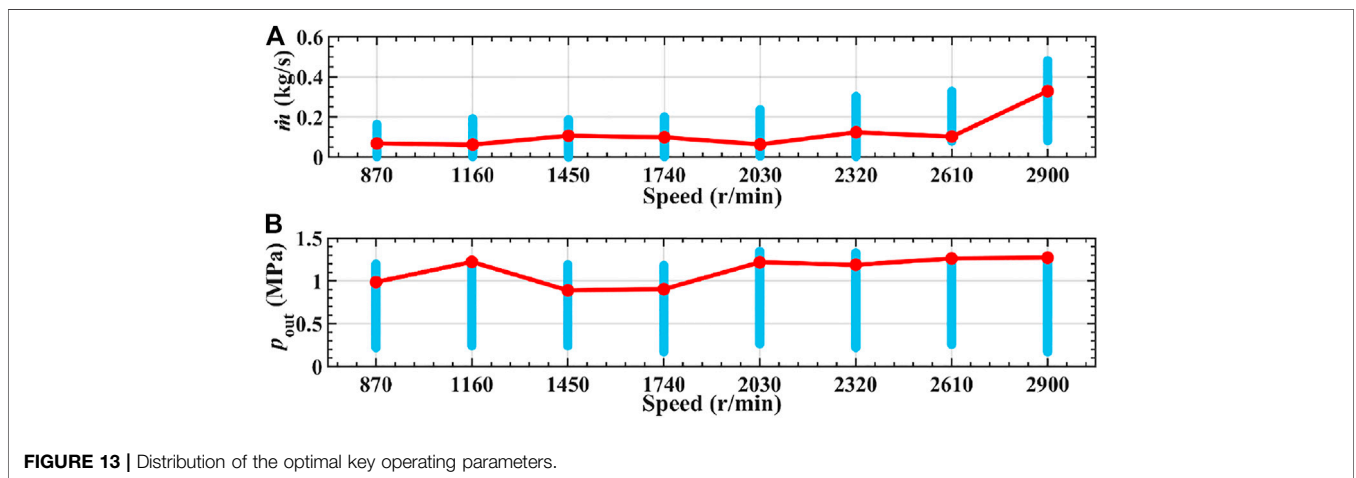
Figure 11 shows the comparison results. Under the same speed and the same operating parameters, the maximum mean absolute percentage error (MAPE) of theoretical analysis is 74.19%, while the machine learning MAPE is only 9.23%. From the figure, compared with the theoretical analysis, machine learning has obvious advantages. In addition, theoretical analysis shows that the optimal inlet temperature is higher than the optimal outlet temperature at the other seven speeds except 2900 r/min. This is completely different from the 21,193 sets of experimental data collected at seven speeds. This is because theoretical analysis has limitations in constructing a true nonlinear mapping relationship between the inlet temperature and outlet temperature. Figure 12 shows the comparison of isentropic efficiency-limiting values. From the figure, the theoretical analysis of the MAPE at 870–2900 r/min is $7.73 \times 10^{-7} - 1.43 \times 10^{-10}\%$.



It can be found that the prediction of the isentropic efficiency and optimal operating parameters by machine learning is significantly better than theoretical analysis in terms of accuracy and objectivity.

4.3.4 Optimal Operating Parameters

The operating parameters corresponding to the maximum isentropic efficiency are shown in **Figure 13**. We want to analyze the position of the optimal operating parameters within the experimental boundary by optimizing the results so as to analyze the coupling relationship between the limiting value of the isentropic efficiency and the optimal operating parameters. The blue bar shows the range of experimental values of operating parameters at different speeds. The red line is the position of the optimal operating parameters at



different speeds. From **Figure 13A**, the optimal mass flow rate is maintained in a low range within the operating parameter boundaries; as the speed increases, although the optimal mass flow rate has been maintained in the low range within the operating parameter boundaries, it generally shows a tendency to move to the middle. It can be seen from **Figure 13B** that the optimal outlet pressure is maintained in a high range within the operating parameter boundaries under different working conditions. With the increase of speed, although the optimal outlet pressure position fluctuates slightly, it has been maintained in the high range of the operating parameter boundaries. In the high-speed range, as the speed increases, the optimal outlet pressure changes mildly. It can be seen that there is no unique set of speed and optimal operating parameters to make the isentropic efficiency reach the limiting value in the full working conditions. However, there is a relatively stable outlet pressure in the high-speed range to make the isentropic efficiency reach the limiting value.

It can be seen from **Table 4**, **Figure 13**, and the operating parameter boundaries that in the low-speed range, it is easier to obtain higher isentropic efficiency by maintaining a low outlet temperature and high outlet pressure. In the high-speed range, it is easier to obtain higher isentropic efficiency by maintaining moderate inlet temperature, moderate outlet temperature, lower inlet pressure, higher outlet pressure, lower mass flow, and moderate power consumption.

This is because the low inlet pressure and high outlet pressure can form a large pressure difference. As the pressure difference increases, the more effective the work, the higher will be the isentropic efficiency. For the hydraulic diaphragm metering pump, the outlet pressure has little effect on mass flow. The ideal flow rate can be obtained by adjusting the speed. The pressure difference and mass flow rate jointly determine the power consumption of the hydraulic diaphragm metering pump. The higher temperature difference between the inlet and outlet of the working fluid pump will lead to the increase of exergy destruction of the pump, which is not conducive to higher isentropic efficiency.

5 CONCLUSION

This study introduces the scatter plot analysis method to analyze the time-varying characteristics of the key operating parameters of the hydraulic diaphragm metering pump. Then, using the bilinear interpolation algorithm, the coupling characteristics and nonlinear change trend between the key parameters and the isentropic efficiency are analyzed. A hybrid model of the machine learning-fitting algorithm is constructed to solve and verify the actual matching correlation equation of the key operating parameters. In addition, a machine learning framework with an intelligent algorithm is constructed. Through the theoretical analysis model, the validity of the framework is compared and verified. Finally, the isentropic efficiency limiting and optimal cycle parameters are evaluated. The main conclusions are summarized as follows:

- 1) It is reasonable to integrate machine learning, intelligent algorithm, and data-driven to build a machine learning framework with an intelligent algorithm and then optimize the maximum isentropic efficiency. The RMSE is 1.8×10^{-3} – 3.8×10^{-2} , and the model has excellent robustness and generalization ability. In addition, the prediction and optimization capabilities of the machine learning framework with the intelligent algorithm for isentropic efficiency are significantly better than the theoretical analysis in accuracy and objectivity.
- 2) There is no unique set of speed and operating parameters to make the isentropic efficiency reach the maximum value under all working conditions. By reasonably adjusting the operating parameters, the isentropic efficiency can reach a larger value under different working conditions. Through reasonable optimization, the limiting value of isentropic efficiency is stable between 70.22 and 74.67% under full working conditions.
- 3) The outlet pressure and mass flow rate can be used as time series variables. The constructed machine learning-fitting algorithm hybrid model can accurately solve and verify the actual matching correlation equation of the key operating parameters. The actual matching correlation equation of the operating parameters between the outlet pressure and mass flow rate is as follows:

$$\dot{m} = 2 - 2 \cos[10 \arcsin(2p_{\text{out}}) - 9] + 10^{-1} \sin[10 \arcsin(2p_{\text{out}}) - 9].$$
- 4) Among the outlet pressure, mass flow rate, inlet pressure, inlet temperature, outlet temperature, and power consumption, the outlet pressure has the greatest impact on the isentropic efficiency. Although under full working conditions, there is no unique set of speed and operating parameters to make the isentropic efficiency reach the limiting value. However, there is a relatively stable outlet pressure in the high-speed range to make the isentropic efficiency reach the limiting value.

This work mainly focuses on the influence of thermodynamic cycle parameters on the isentropic efficiency of the working fluid pump. In our future work, we will pay more attention to the influence of transient pulsation of mass flow on the power output of the expander.

DATA AVAILABILITY STATEMENT

The original contributions presented in the study are included in the article/Supplementary Material, further inquiries can be directed to the corresponding author.

AUTHOR CONTRIBUTIONS

XP: investigation, conceptualization, methodology, software, validation, and writing—original draft. BY: conceptualization,

methodology, writing—review and editing, and supervision. KN: conceptualization, methodology, and writing—review and editing. MY: conceptualization, methodology, and writing—review and editing.

REFERENCES

- Altun, A. F., and Kilic, M. (2020). Thermodynamic Performance Evaluation of a Geothermal ORC Power Plant. *Renew. Energy* 148, 261–274. doi:10.1016/j.renene.2019.12.034
- Carraro, G., Bori, V., Lazzaretto, A., Toniato, G., and Danielli, P. (2020). Experimental Investigation of an Innovative Biomass-Fired Micro-ORC System for Cogeneration Applications. *Renew. Energy* 161, 1226–1243. doi:10.1016/j.renene.2020.07.012
- Chang, J.-C., Hung, T.-C., He, Y.-L., and Zhang, W. (2015). Experimental Study on Low-Temperature Organic Rankine Cycle Utilizing Scroll Type Expander. *Appl. Energy* 155, 150–159. doi:10.1016/j.apenergy.2015.05.118
- D'Amico, F., Pallis, P., Leontaritis, A. D., Karellas, S., Kakalis, N. M., Rech, S., et al. (2018). Semi-empirical Model of a Multi-Diaphragm Pump in an Organic Rankine Cycle (ORC) Experimental Unit. *Energy* 143, 1056–1071. doi:10.1016/j.energy.2017.10.127
- Feng, Y., Zhang, Y., Li, B., Yang, J., and Shi, Y. (2015). Comparison between Regenerative Organic Rankine Cycle (RORC) and Basic Organic Rankine Cycle (BORC) Based on Thermoeconomic Multi-Objective Optimization Considering Exergy Efficiency and Levelized Energy Cost (LEC). *Energy Convers. Manage.* 96, 58–71. doi:10.1016/j.enconman.2015.02.045
- Feng, Y., Hung, T., Zhang, Y., Li, B., Yang, J., and Shi, Y. (2015). Performance Comparison of Low-Grade ORCs (Organic Rankine Cycles) Using R245fa, Pentane and Their Mixtures Based on the Thermoeconomic Multi-Objective Optimization and Decision Makings. *Energy* 93, 2018–2029. doi:10.1016/j.energy.2015.10.065
- Feng, Y.-q., Hung, T.-C., He, Y.-L., Wang, Q., Chen, S.-C., Wu, S.-L., et al. (2019). Experimental Investigation of Lubricant Oil on a 3 kW Organic Rankine Cycle (ORC) Using R123. *Energy Convers. Manage.* 182, 340–350. doi:10.1016/j.enconman.2018.12.021
- Feng, Y., Du, Z., Shreka, M., Zhu, Y., Zhou, S., and Zhang, W. (2020). Thermodynamic Analysis and Performance Optimization of the Supercritical Carbon Dioxide Brayton Cycle Combined with the Kalina Cycle for Waste Heat Recovery from a marine Low-Speed Diesel Engine. *Energy Convers. Manage.* 206, 112483. doi:10.1016/j.enconman.2020.112483
- Fubin Yang, F., Cho, H., Zhang, H., Zhang, J., and Wu, Y. (2018). Artificial Neural Network (ANN) Based Prediction and Optimization of an Organic Rankine Cycle (ORC) for Diesel Engine Waste Heat Recovery. *Energy Convers. Manage.* 164, 15–26. doi:10.1016/j.enconman.2018.02.062
- Guo, Q., Qi, X., Wei, Z., Yin, Q., Sun, P., Guo, P., et al. (2019). Modeling and Characteristic Analysis of Fouling in a Wet Cooling tower Based on Wavelet Neural Networks. *Appl. Therm. Eng.* 152, 907–916. doi:10.1016/j.applthermaleng.2019.02.041
- Hamedani, M. H., Sadeghian, H., Zekri, M., Sheikholeslam, F., and Keshmiri, M. (2021). Intelligent Impedance Control Using Wavelet Neural Network for Dynamic Contact Force Tracking in Unknown Varying Environments. *Control. Eng. Pract.* 113, 104840. doi:10.1016/j.conengprac.2021.104840
- Hop, D. C., Van Hop, N., and Anh, T. T. M. (2021). Adaptive Particle Swarm Optimization for Integrated Quay crane and Yard Truck Scheduling Problem. *Comput. Ind. Eng.* 153, 107075. doi:10.1016/j.cie.2020.107075
- Hu, Y., Li, J., Hong, M., Ren, J., Lin, R., Liu, Y., et al. (2019). Short Term Electric Load Forecasting Model and its Verification for Process Industrial Enterprises Based on Hybrid GA-PSO-BPNN Algorithm-A Case Study of Papermaking Process. *Energy* 170, 1215–1227. doi:10.1016/j.energy.2018.12.208
- Jafari, S., Khalilary, S., Shwabkeh, A., Wae-hayee, M., and Hashemian, M. (2021). A Complete Energetic and Exergetic Analysis of a Solar Powered Trigenation System with Two Novel Organic Rankine Cycle (ORC) Configurations. *J. Clean. Prod.* 281, 124552. doi:10.1016/j.jclepro.2020.124552
- Jafarzadeh Ghouschi, S., Manjili, S., Mardani, A., and Saraji, M. K. (2021). An Extended New Approach for Forecasting Short-Term Wind Power Using Modified Fuzzy Wavelet Neural Network: A Case Study in Wind Power Plant. *Energy* 223, 120052. doi:10.1016/j.energy.2021.120052
- Khoshgoftar Manesh, M. H., Firouzi, P., Kabiri, S., and Blanco-Marigorta, A. M. (2021). Evaluation of Power and Freshwater Production Based on Integrated Gas Turbine, S-CO₂, and ORC Cycles with RO Desalination Unit. *Energy Convers. Manage.* 228, 113607. doi:10.1016/j.enconman.2020.113607
- Kim, D. K., Lee, J. S., Kim, J., Kim, M. S., and Kim, M. S. (2017). Parametric Study and Performance Evaluation of an Organic Rankine Cycle (ORC) System Using Low-Grade Heat at Temperatures below 80 °C. *Appl. Energy* 189, 55–65. doi:10.1016/j.apenergy.2016.12.026
- Kosmadakis, G., Landelle, A., Lazova, M., Manolakis, D., Kaya, A., Huisseune, H., et al. (2016). Experimental Testing of a Low-Temperature Organic Rankine Cycle (ORC) Engine Coupled with Concentrating PV/thermal Collectors: Laboratory and Field Tests. *Energy* 117, 222–236. doi:10.1016/j.energy.2016.10.047
- Li, W., Mckeown, A., and Yu, Z. (2020). Correction of Cavitation with Thermodynamic Effect for a Diaphragm Pump in Organic Rankine Cycle Systems. *Energy Rep.* 6, 2956–2972. doi:10.1016/j.egy.2020.10.013
- Mateu-Royo, C., Mota-Babiloni, A., Navarro-Esbrí, J., Peris, B., Molés, F., and Amat-Albuixech, M. (2019). Multi-objective Optimization of a Novel Reversible High-Temperature Heat Pump-Organic Rankine Cycle (HTHP-ORC) for Industrial Low-Grade Waste Heat Recovery. *Energy Convers. Manage.* 197, 111908. doi:10.1016/j.enconman.2019.111908
- Meng, F., Zhang, H., Yang, F., Hou, X., Lei, B., Zhang, L., et al. (2017). Study of Efficiency of a Multistage Centrifugal Pump Used in Engine Waste Heat Recovery Application. *Appl. Therm. Eng.* 110, 779–786. doi:10.1016/j.applthermaleng.2016.08.226
- Miao, Z., Xu, J., Yang, X., and Zou, J. (2015). Operation and Performance of a Low Temperature Organic Rankine Cycle. *Appl. Therm. Eng.* 75, 1065–1075. doi:10.1016/j.applthermaleng.2014.10.065
- Mohammadzadeh Bina, S., Jalilinasrabad, S., and Fujii, H. (2017). Thermoeconomic Evaluation of Various Bottoming ORCs for Geothermal Power Plant, Determination of Optimum Cycle for Sabalan Power Plant Exhaust. *Geothermics* 70, 181–191. doi:10.1016/j.geothermics.2017.06.007
- Morais, P. H. d. S., Lodi, A., Aoki, A. C., and Modesto, M. (2020). Energy, Exergetic and Economic Analyses of a Combined Solar-Biomass-ORC Cooling Cogeneration Systems for a Brazilian Small Plant. *Renew. Energy* 157, 1131–1147. doi:10.1016/j.renene.2020.04.147
- Nematollahi, O., Abadi, G. B., Kim, D. Y., and Kim, K. C. (2018). Experimental Study of Brazed Compact Metal-Foam Evaporator in an Organic Rankine Cycle Performance: Toward a Compact ORC. *Energy Convers. Manage.* 173, 37–45. doi:10.1016/j.enconman.2018.07.071
- Palagi, L., Pesyridis, A., Sciubba, E., and Tocci, L. (2019). Machine Learning for the Prediction of the Dynamic Behavior of a Small Scale ORC System. *Energy* 166, 72–82. doi:10.1016/j.energy.2018.10.059
- Peris, B., Navarro-Esbrí, J., Molés, F., Martí, J. P., and Mota-Babiloni, A. (2015). Experimental Characterization of an Organic Rankine Cycle (ORC) for Micro-scale CHP Applications. *Appl. Therm. Eng.* 79, 1–8. doi:10.1016/j.applthermaleng.2015.01.020
- Ping, X., Yang, F., Zhang, H., Zhang, W., Song, G., and Yang, Y. (2020). Prediction and Optimization of Isentropic Efficiency of Vortex Pump under Full Operating Conditions in Organic Rankine Cycle Waste Heat Recovery System Based on Deep Learning and Intelligent Algorithm. *Sustainable Energy Tech. Assessments* 42, 100898. doi:10.1016/j.seta.2020.100898
- Ping, X., Yang, F., Zhang, H., Zhang, J., Zhang, W., and Song, G. (2021). Introducing Machine Learning and Hybrid Algorithm for Prediction and Optimization of Multistage Centrifugal Pump in an ORC System. *Energy* 222, 120007. doi:10.1016/j.energy.2021.120007
- Ping, X., Yao, B., Zhang, H., and Yang, F. (2021). Thermodynamic Analysis and High-Dimensional Evolutionary many-objective Optimization of Dual Loop

ACKNOWLEDGMENTS

The authors would like to thank the reviewers for their valuable comments on this research.

- Organic Rankine Cycle (DORC) for CNG Engine Waste Heat Recovery. *Energy* 236, 121508. doi:10.1016/j.energy.2021.121508
- Ping, X., Yao, B., Zhang, H., and Yang, F. (2021). Thermodynamic, Economic, and Environmental Analysis and Multi-Objective Optimization of a Dual Loop Organic Rankine Cycle for CNG Engine Waste Heat Recovery. *Appl. Therm. Eng.* 193, 116980. doi:10.1016/j.applthermaleng.2021.116980
- Ping, X., Yang, F., Zhang, H., Zhang, W., Zhang, J., Song, G., et al. (2021). Prediction and Optimization of Power Output of Single Screw Expander in Organic Rankine Cycle (ORC) for Diesel Engine Waste Heat Recovery. *Appl. Therm. Eng.* 182, 116048. doi:10.1016/j.applthermaleng.2020.116048
- Rossi, M., and Renzi, M. (2018). A General Methodology for Performance Prediction of Pumps-As-Turbines Using Artificial Neural Networks. *Renew. Energy* 128, 265–274. doi:10.1016/j.renene.2018.05.060
- Roumpedakis, T. C., Christou, T., Monokrousou, E., Braimakis, K., and Karellas, S. (2019). Integrated ORC-Adsorption Cycle: A First and Second Law Analysis of Potential Configurations. *Energy* 179, 46–58. doi:10.1016/j.energy.2019.04.069
- Santhosh, M., Venkaiah, C., and Vinod Kumar, D. M. (2018). Ensemble Empirical Mode Decomposition Based Adaptive Wavelet Neural Network Method for Wind Speed Prediction. *Energy Convers. Manage.* 168, 482–493. doi:10.1016/j.enconman.2018.04.099
- Schifflechner, C., Dawo, F., Eyerer, S., Wieland, C., and Spliethoff, H. (2020). Thermodynamic Comparison of Direct Supercritical CO₂ and Indirect Brine-ORC Concepts for Geothermal Combined Heat and Power Generation. *Renew. Energy* 161, 1292–1302. doi:10.1016/j.renene.2020.07.044
- Shen, G. F., Yuan, F., Li, Y., and Liu, W. (2019). The Energy Flow Method for Modeling and Optimization of Organic Rankine Cycle (ORC) Systems. *Energy Convers. Manage.* 199, 11958. doi:10.1016/j.enconman.2019.111958
- Taherkhani, M., and Safabakhsh, R. (2016). A Novel Stability-Based Adaptive Inertia Weight for Particle Swarm Optimization. *Appl. Soft Comput.* 38, 281–295. doi:10.1016/j.asoc.2015.10.004
- Uusitalo, A., Turunen-Saaresti, T., Honkatukia, J., and Dhanasegaran, R. (2020). Experimental Study of Small Scale and High Expansion Ratio ORC for Recovering High Temperature Waste Heat. *Energy* 208, 118321. doi:10.1016/j.energy.2020.118321
- Villani, M., and Tribioli, L. (2019). Comparison of Different Layouts for the Integration of an Organic Rankine Cycle Unit in Electrified Powertrains of Heavy Duty Diesel Trucks. *Energy Convers. Manage.* 187, 248–261. doi:10.1016/j.enconman.2019.02.078
- Wang, S., and Fu, Z. (2019). Thermodynamic and Economic Analysis of Solar Assisted CCHP-ORC System with DME as Fuel. *Energy Convers. Manage.* 186, 535–545. doi:10.1016/j.enconman.2019.02.076
- Wang, X. D., Zhao, L., Wang, J. L., Zhang, W. Z., Zhao, X. Z., and Wu, W. (2010). Performance Evaluation of a Low-Temperature Solar Rankine Cycle System Utilizing R245fa. *Solar Energy* 84, 353–364. doi:10.1016/j.solener.2009.11.004
- Wang, E., Yu, Z., Zhang, H., and Yang, F. (2017). A Regenerative Supercritical-Subcritical Dual-Loop Organic Rankine Cycle System for Energy Recovery from the Waste Heat of Internal Combustion Engines. *Appl. Energy* 190, 574–590. doi:10.1016/j.apenergy.2016.12.122
- Wang, E., Yu, Z., and Collings, P. (2017). Dynamic Control Strategy of a Distillation System for a Composition-Adjustable Organic Rankine Cycle. *Energy* 141, 1038–1051. doi:10.1016/j.energy.2017.09.141
- Wang, T., Liu, L., Zhu, T., and Gao, N. (2019). Experimental Investigation of a Small-Scale Organic Rankine Cycle under Off-Design Conditions: From the Perspective of Data Fluctuation. *Energy Convers. Manage.* 198, 111826. doi:10.1016/j.enconman.2019.111826
- Wang, G., Awad, O. I., Liu, S., Shuai, S., and Wang, Z. (2020). NO_x Emissions Prediction Based on Mutual Information and Back Propagation Neural Network Using Correlation Quantitative Analysis. *Energy* 198, 117286. doi:10.1016/j.energy.2020.117286
- Wang, F., Wang, L., Zhang, H., Xia, L., Miao, H., and Yuan, J. (2021). Design and Optimization of Hydrogen Production by Solid Oxide Electrolyzer with marine Engine Waste Heat Recovery and ORC Cycle. *Energy Convers. Manage.* 229, 113775. doi:10.1016/j.enconman.2020.113775
- Wang, E., Zhang, M., Meng, F., and Zhang, H. (2022). Zeotropic Working Fluid Selection for an Organic Rankine Cycle Bottoming with a marine Engine. *Energy* 243, 123097. doi:10.1016/j.energy.2021.123097
- Wu, X., Li, C., Jia, W., and He, Y. (2014). Optimal Operation of Trunk Natural Gas Pipelines via an Inertia-Adaptive Particle Swarm Optimization Algorithm. *J. Nat. Gas Sci. Eng.* 21, 10–18. doi:10.1016/j.jngse.2014.07.028
- Xie, Y., Hu, P., Zhu, N., Lei, F., Xing, L., Xu, L., et al. (2020). A Hybrid Short-Term Load Forecasting Model and its Application in Ground Source Heat Pump with Cooling Storage System. *Renew. Energy* 161, 1244–1259. doi:10.1016/j.renene.2020.07.142
- Xu, Y., Zhang, H., Yang, F., Tong, L., Yang, Y., Yan, D., et al. (2021). Experimental Study on Small Power Generation Energy Storage Device Based on Pneumatic Motor and Compressed Air. *Energy Convers. Manage.* 234, 113949. doi:10.1016/j.enconman.2021.113949
- Yuan, Z., Wang, W., Wang, H., and Mizzi, S. (2020). Combination of Cuckoo Search and Wavelet Neural Network for Midterm Building Energy Forecast. *Energy* 202, 117728. doi:10.1016/j.energy.2020.117728
- Yuxin Yang, Y., Zhang, H., Xu, Y., Zhao, R., Hou, X., and Liu, Y. (2018). Experimental Study and Performance Analysis of a Hydraulic Diaphragm Metering Pump Used in Organic Rankine Cycle System. *Appl. Therm. Eng.* 132, 605–612. doi:10.1016/j.applthermaleng.2018.01.001
- Zhao, M., Canova, M., Tian, H., and Shu, G. (2019). Design Space Exploration for Waste Heat Recovery System in Automotive Application under Driving Cycle. *Energy* 176, 980–990. doi:10.1016/j.energy.2019.04.063

Conflict of Interest: The authors declare that the research was conducted in the absence of any commercial or financial relationships that could be construed as a potential conflict of interest.

Publisher's Note: All claims expressed in this article are solely those of the authors and do not necessarily represent those of their affiliated organizations, or those of the publisher, the editors, and the reviewers. Any product that may be evaluated in this article, or claim that may be made by its manufacturer, is not guaranteed or endorsed by the publisher.

Copyright © 2022 Ping, Yao, Niu and Yuan. This is an open-access article distributed under the terms of the Creative Commons Attribution License (CC BY). The use, distribution or reproduction in other forums is permitted, provided the original author(s) and the copyright owner(s) are credited and that the original publication in this journal is cited, in accordance with accepted academic practice. No use, distribution or reproduction is permitted which does not comply with these terms.